JTTEE5 15:53-62
DOI: 10.1361/105996306X92596
1059-9630/$19.00 © ASM International

Relationships Between Microstructure and Electrical Properties of RF and DC Plasma-Sprayed Titania Coatings

N. Branland, E. Meillot, P. Fauchais, A. Vardelle, F. Gitzhofer, and M. Boulos

(Submitted February 22, 2005; in revised form October 16, 2005)

Relationships between electrical properties of thermally sprayed titania coatings and their microstructures have been investigated. It is well known that the quality and properties of the plasma-sprayed coatings are strongly dependent on the in-flight particle characteristics, which directly influences the plasma-sprayed coating microstructures. As far as possible, a broad range of microstructures was produced by using various processes of plasma spraying with different powder size ranges and variation of the plasma operating parameters. The two plasma-spraying processes consisted of direct current (DC) and radio frequency (RF) plasma spraying. The major concern of the study was that plasma-sprayed parameters influence also the stoichiometry of the titania coating resulting in a large variation of their electrical properties. It is the reason why coatings with identical stoichiometry were compared. The comparison between RF and DC plasma-sprayed titania coatings highlighted that electrical resistivity was directly linked to the quality of the contact between the splats and their density through the titania plasma-sprayed coatings.

Keywords DC plasma spraying, electrical resistivity, microstructure, particle characteristics at impact, RF plasma spraying, stoichiometry, titania

1. Introduction

In plasma spraying, coatings are formed by the layering of molten or semimolten particles, projected by the plasma, that impact and flatten on a prepared substrate (Ref 1), where they solidify within a few microseconds, forming splats. Therefore, coating properties strongly depend on the quality of the contact established between the substrate and layered splats, the size and morphology of pores, the possible crack network, and other coating defects. For instance, in plasma-sprayed zirconia coatings, an increase in the contact area between splats from 17 to 35% leads to an increase of the coating thermal diffusivity from 1.9×10^{-7} to 3.6×10^{-7} m^2 s^{-1} (Ref 2). The relationships between thermal properties of plasma-sprayed coatings and their microstructures have been the subject of numerous studies (Ref 3, 4), whereas the parallel electrical property-microstructure relationships have not been so vigorously studied and the main objective of this present paper is to establish the link between electrical properties of titania plasma-sprayed coatings and their microstructures.

Electrical properties are due to the transport of electrons, holes, ions, and point defects through the area of good contact between splats. Usually, ions and defects are the charge carriers active in ceramics. At elevated temperatures, electrons that are thermally excited across the energy gap also contribute to electrical conduction processes. In plasma-sprayed titania coatings, point defects play a major role in their electrical conduction. Indeed, when titanium dioxide is plasma-treated and reaches temperatures near the melting point, oxygen vacancies are formed in the flattening droplets (Ref 5). These point defects act as donor centers and change the original insulating rutile into an n-type semiconductor. This change is accompanied with changes in the coating color from white to gray-black. It has been experimentally observed that the operating conditions of the plasma spray process can affect the stoichiometric composition of the coatings and, therefore, their electrical properties (Ref 6, 7).

In this study, two plasma spray processes have been compared to obtain a better understanding of the correlation between the microstructures and electrical properties of coatings. These spray processes are the direct current plasma spraying at atmospheric pressure (atmospheric plasma spraying [APS]) and the

N. Branland and **E. Meillot,** CEA Le Ripault, BP 16, 37260 Monts, France; **P. Fauchais** and **A. Vardelle,** SPCTS, University of Limoges, 123 av. A. Thomas, 87000 Limoges, France; and **F. Gitzhofer** and **M. Boulos,** CRTP, University of Sherbrooke, Sherbrooke, Quebec, Canada J1K 2R1. Contact e-mail: fauchais@unilim.fr.

Nomenclature

APS	atmospheric plasma spraying
CL	cathodoluminescence
CLSM	confocal laser scanning microscopy
DC	direct current
IPS	inductive plasma spraying
L	lightness value
M	Magneli phase
P	open porosity
RF	radio frequency
T_m	melting point of TiO_2
α	linear coefficient of thermal expansion
ρ	electrical resistivity

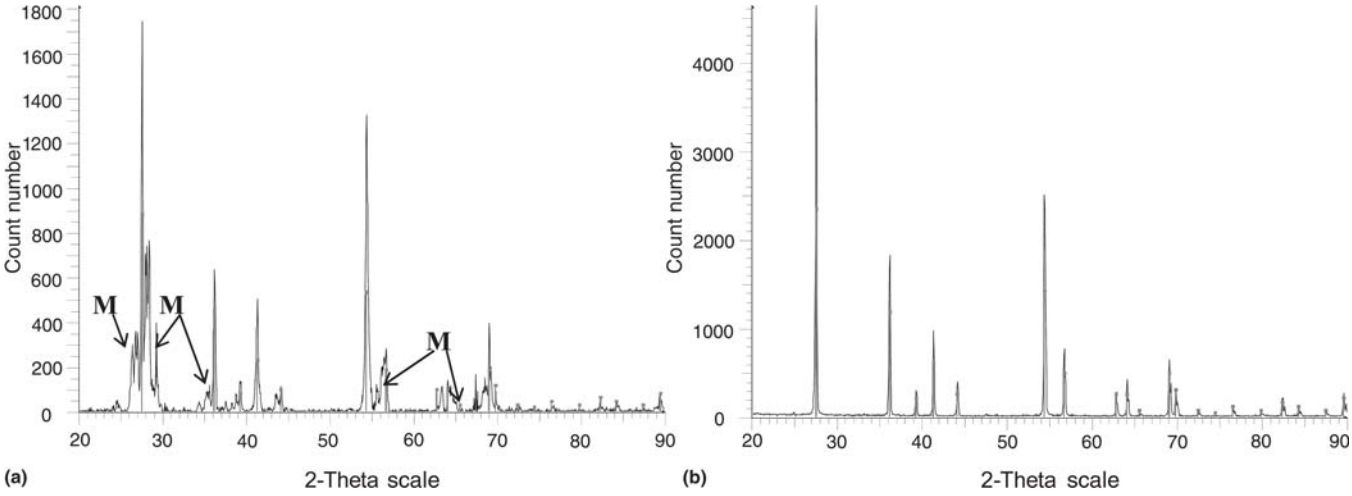

Fig. 1 XRD patterns of (a) the raw TiO_2 powder and (b) the heat-treated TiO_2 powder at 1000 °C during 3 h (XRD peaks correspond to rutile JCPDS card 21-1276, M = Magneli phases)

inductive plasma spraying (IPS) operating in either subsonic or supersonic mode. The deposition processes lead to different coating microstructures due to the difference in the melting state and velocity of particles at impact on the substrate (Ref 8). In IPS running in subsonic mode, particle velocities prior to impact are about five to ten times lower than those involved in APS, and this results in a more marked "lamellar" morphology (Ref 9); in supersonic mode (Ref 10), IPS leads to particle velocities that are equal to and even higher than the particle velocities obtained systematically in the APS process (Ref 11). For the APS and IPS spray tests, the main operating parameters were varied to obtain a wide range of particle characteristics prior to their impact on the substrate.

The first part of this paper is devoted to the study of the relationships between some plasma parameters and particle characteristics at point of impact. In the second part, the effects of particle characteristics on coating properties are discussed. Finally, the last part deals with the electrical properties of titania plasma-sprayed coatings. In this study, the stoichiometry of coatings was evaluated mainly with titania's characteristic of changing color with structural oxygen depletion.

2. Experimental Procedures and Coating Characterization

2.1 Materials

The titania materials used in this investigation were commercially available TiO_2 powders. The particle size distributions were selected so that they were appropriate for each of the spraying processes used. In all cases, the powder exhibited rutile and Magneli structures (Ti_nO_{2n-1} with n = 4-10). Consequently, before spraying, powders were annealed at 1000 °C in air for a period of 3 h. After this treatment, their structure became that of the pure rutile phase. The x-ray diffraction (XRD) patterns of the raw powder and the corresponding heat-treated powder are presented in Fig. 1.

The substrate conditions are well known to contribute to the qualities of coating formation (Ref 12). However, in this study, they were kept constant to evaluate only the effect of the particle characteristics on coating microstructures. To limit the formation of expansion mismatch stresses, the stainless steel substrate material (X13M) had a linear coefficient of thermal expansion ($\alpha_{substrate} = 10.7 \times 10^{-6}\ °C^{-1}$) close to that of rutile ($\alpha_{TiO2} = 8.8 \times 10^{-6}\ °C^{-1}$). The substrates, 25 mm in diameter and 5 mm thick, were prepared by grit blasting and degreasing before spraying. Grit blasting was performed with a suction type machine at a pressure of 0.7 MPa, a nozzle internal diameter (i.d.) of 8 mm, a blasting distance of 100 mm, and using alumina grit with a mean particle diameter of 1 mm. The resulting substrate Ra was 7 μm.

The substrate temperature was maintained at 200 °C during APS deposition. This temperature was chosen because a separate study of the substrate temperature effect on splat formation revealed that, at this temperature, disk-like splats of evenly distributed thickness could be formed when molten droplets were flattened by impact onto the flat substrate (Ra ≈ 0.1 μm) (Ref 13). Unfortunately, in the IPS installation, it was impossible to maintain the substrate temperature at a constant value. Therefore, the deposition temperature varied between 400 and 500 °C depending on the varying operating conditions of the spray process.

2.2 Plasma Conditions

In the APS tests, to limit the deoxidation of the TiO_2 particles during the deposition process, hydrogen was not used as a plasma gas: a Sulzer Metco torch (F4VB) (Wohlen, Switzerland) was operated with an argon-helium gas mixture. The powder was injected radially downstream of the nozzle exit at a constant feed rate (20 g/min). The carrier gas (argon) flow rate was adjusted in such a way that the particles mean trajectory in the plasma jet was optimized with an angle of about 4° relative to the torch axis. The substrate standoff distance was 100 mm. The injector was a stainless steel tube with an inside diameter of 1.8 mm. It was located at 6 mm downstream of the plasma torch exit and at 9 mm from the plasma torch axis.

In the IPS tests, a plasma torch (TEKNA PL-35, Quebec,

Table 1 Spraying processes and spray parameters used for the production of TiO_2 coatings

Spray process and particle size range	Varied parameters	Values
APS 22-45 μm	Effective power input to the gas	11.6 to 23.5 kW
	Secondary gas flow rate	He: 34 to 75 vol%
	Total gas mass flow rate	0.684 to 1.961 g/s
	Plasma torch diameter	6 and 8 mm
IPS subsonic 22-45 μm	Plasma energy	17 to 25 kW
	Spraying distance	150 to 200 mm
	Coil region pressure	53.3 kPa when chamber pressure < 53.3 kPa Otherwise equal to chamber pressure
	Chamber pressure	33.3 to 79.9 kPa
IPS supersonic 5-20 μm	Plasma energy	17 to 25 kW
	Spraying distance	200 to 220 mm
	Coil region pressure	53.3 kPa
	Chamber pressure	3.3 to 13.3 kPa

Canada), with a ceramic plasma confinement tube of 35 mm i.d., was used to produce the TiO_2 coatings. A vacuum pump made it possible to maintain the pressure, p, in the deposition chamber at the desired level (3.99 kPa < p < 79.9 kPa). In the subsonic mode, the powder was injected axially into the plasma through a water-cooled stainless steel probe (internal diameter = 2.5 mm) whose exit tip was located at 40 mm upstream of the exit plane of the torch nozzle. The powder feeding rate was 11 g/min. In supersonic mode, a convergent-divergent nozzle with a critical throat diameter of 10 mm was added to the PL35 torch. The powder feed rate and the probe position were 3.5 g/min and 90 mm upstream of the exit plane of the torch nozzle, respectively.

In both modes (subsonic and supersonic), the absence of electrodes in the spraying process allowed the use of oxygen (70 slpm) as the sheath gas to limit the in-flight reduction of titania particles. The plasma (central) and powder carrier gases were pure argon with flow rates used equal to 40 and 4 slpm, respectively.

For both spray processes, the operating parameters (listed in Table 1) were varied to obtain a wide range of spray particle characteristics at impact and, therefore, to produce coatings with different properties.

2.3 In-Flight Particle Characterization

In-flight particle temperature and velocity were measured using a DPV-2000 diagnostic system (Tecnar Automation Ltd., Quebec, Canada). The surface temperature was determined by two-color pyrometry and the velocity by time-of-flight between mask slits. This measuring system possesses an analyzed volume between 0.3 and 0.6 mm^3. The measurement accuracy was estimated to be about 5% for particle velocity and 20% for particle temperature (Ref 14). Measurements were performed without substrate but sited at the standoff distance for coating deposition on substrates.

In the APS tests, the standoff distance for the DPV-2000 sensor was fixed at 100 mm downstream from the exit plane of the torch. For each set of process parameters, the sensor head was manually autocentered with a micrometric table in the region of maximum particle flow.

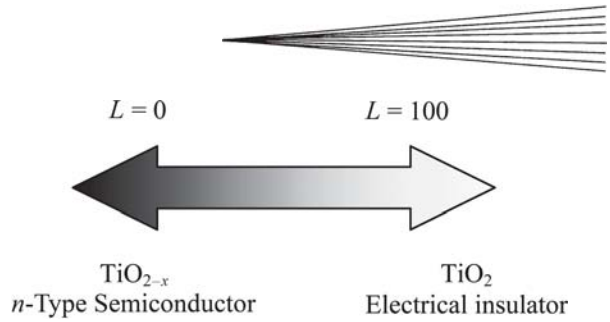

Fig. 2 Relationship between the electrical behavior of TiO_2 coatings and their color lightness

In IPS, the sensor head was centered on the axis of the torch at the various locations of the substrate.

2.4 Metallography and Microscopy

Because mechanical stresses may arise during the mounting, cutting, grinding, and polishing operations of samples, the metallographic preparation procedures can lead to material pull-out, thus altering structural features and damaging the specimen (Ref 15). Therefore, coatings have been strengthened by impregnation under vacuum with epoxy resin (Spurr-Sigma and Fluka, Lyon, France) and cured for 12 h at 80 °C. The advantage of this resin is its very low viscosity (6×10^{-2} Pa s) (Ref 16) that makes it possible for it to efficiently penetrate the plasma-sprayed coatings and so, strengthen their structure. Fluorescent dye (Epodye-Struers, Marne Cedex, France) was also added to observe the coating microstructure by means of a confocal laser scanning microscope (CLSM) (Ref 17). The same procedures for the cutting and polishing operations were carefully followed for all of the samples.

2.5 Porosimetry

The open porosity and apparent density were determined by a water-immersion method, and the pore size distribution was measured using a standard mercury-intrusion method (Ref 18).

2.6 Stoichiometry Determination

Over the full range of spraying parameters used in this investigation, gray-colored titania coatings were invariably obtained, the coloration indicating that coatings were oxygen deficient. To examine the qualitative influence of spraying parameters on the coating stoichiometry, coating color measurements were carried out with the CIELAB colorimetry system (Ref 19). The measured parameter was the lightness value L (Fig. 2), which can vary from 0 to 100. The value 0 corresponds to the absence of color (i.e., a black coating), and the value 100 corresponds to a white coating.

A quantitative determination of the coating stoichiometry was also made for the APS coatings. It consisted of annealing the coatings at 1000 °C in air for 25 h and then estimating the [O]/[Ti] ratio from the difference in coating weights before and after the thermal treatment.

2.7 Electrical Resistivity Measurements

A four-point method was used to measure the electrical resistivity of TiO_2 coatings perpendicularly to the substrate (Ref

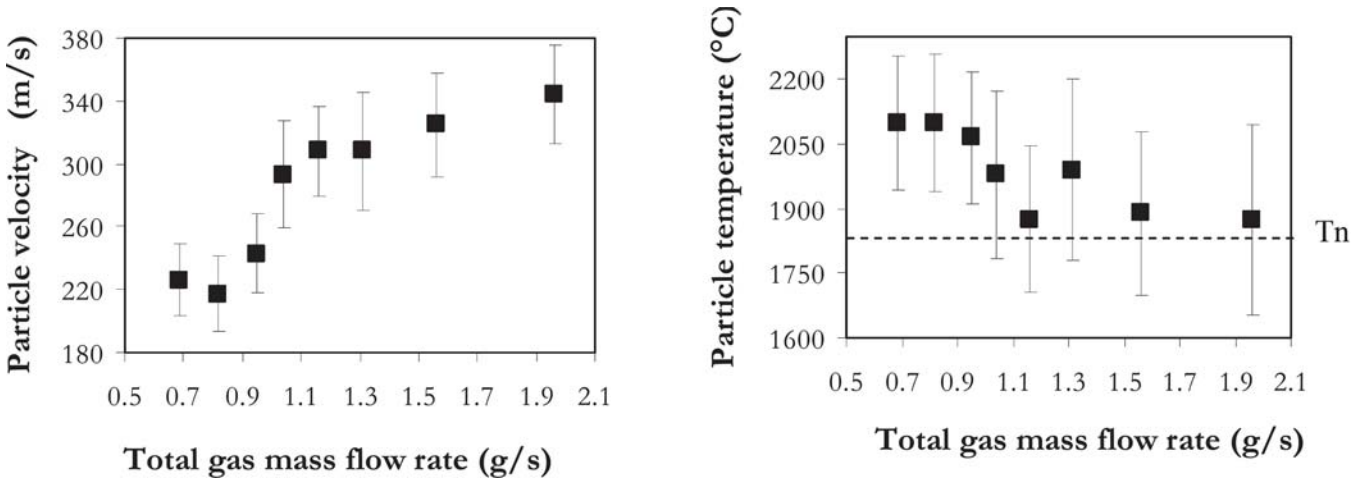

Fig. 3 Variation of the mean particle velocity and temperature with the total gas mass flow rate (melting point of TiO_2, $T_m \approx 1850$ °C)

20). To eliminate the effect of the metallic substrate, each coating was removed from its supporting substrate by dissolving the latter in aqua regia (HCl, HNO_3, and water).

3. Results and Discussion

3.1 Relationship Between Process Parameters and Particle Characteristics at Impact

In both plasma processes, the variation of the operating parameters presented in Table 1 led to a broad range of particle characteristics on impact that included velocity and temperature but also oxygen depletion of titania particles at impact. The effect of the plasma parameters on in-flight particle behavior has been described in detail elsewhere (Ref 21); therefore, only the effects of total gas mass flow rate in APS and chamber pressure in IPS are discussed in this paper.

In APS, with a torch nozzle internal diameter of 6 mm, the variation of the gas mass flow rate from 0.684 to 1.961 g/s permitted particle velocities varying from 215 to 345 m/s to be obtained. In fact, an increase in plasma-gas mass flow rate involves an increase in the plasma jet velocity with the dissipated power, which contributes to the increased particle velocity (Ref 22). On the other hand, this rise of velocity by 52% resulted in a decrease in particle residence time in the plasma jet involving a lower temperature at impact (as shown in Fig. 3).

In IPS, whatever the operating mode (subsonic or supersonic), the most influential parameter is the pressure maintained in the deposition chamber. In fact, the chamber pressure affects the plasma discharge volume and length and, consequently, the particle residence time in the plasma flow.

In IPS-subsonic mode (Fig. 4), the increase in chamber pressure results in decreased particle velocities and, consequently, increased residence time in the plasma plume.

In fact, the length of the plasma plume decreases with increased chamber pressure, due to the braking force exerted by the surroundings on the plasma discharge. Therefore, the momentum transfer between plasma and particles is weakened, leading to reduced particle velocities.

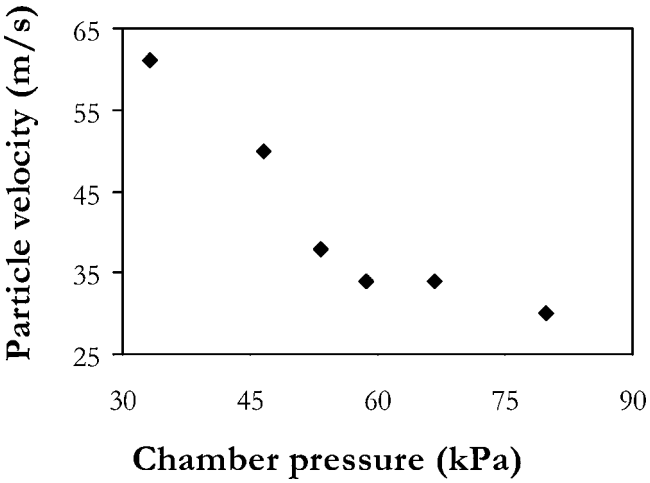

Fig. 4 Variation of the mean particle velocity with the chamber pressure in IPS-subsonic mode

In IPS operating under supersonic mode conditions, the effect of chamber pressure was similar (Fig. 5). Furthermore, decreased chamber pressure enhances the supersonic conditions. Consequently, the lower the chamber pressure, the greater the particle velocities.

Table 2 summarizes particle characteristics obtained for all of the various spraying conditions used in this study.

IPS operating in subsonic mode is characterized by large plasma volumes, low gas velocities, and low energy densities due to the larger torch diameter used (35 mm) compared with that of the APS plasma torch (6 mm). Thus, particles have rather low velocities, ranging from 30 to 60 m/s according to the spraying conditions chosen (Ref 8). The use of a special nozzle for the induction torch makes it possible to work in supersonic mode and obtain particle velocities in the range of 330 to 730 m/s. The comparison between the three plasma processes applied in this study has highlighted their complementarity in terms of the particle velocities achieved.

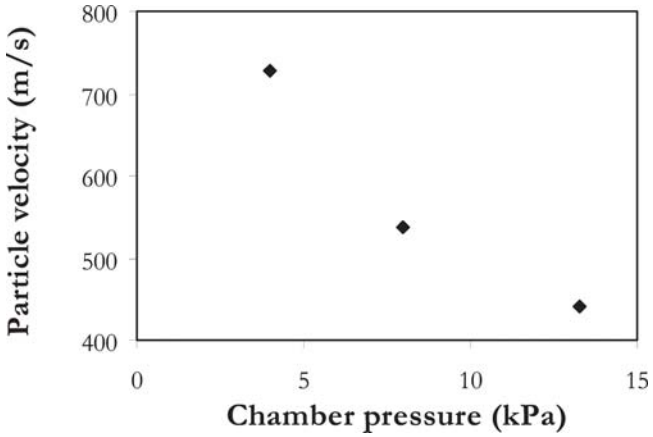

Fig. 5 Variation of the mean particle velocity with the chamber pressure in IPS-supersonic mode

Table 2 Range of the in-flight characteristics of particles according to the plasma-spraying process

		IPS	
	APS	Subsonic	Supersonic
Powder granulometry, μm	22-45	22-45	5-20
Particle temperature, °C	1900-2850	2000-2150	2050-2150
Particle velocity, m/s	140-350	30-60	330-730

3.2 Relationships Between Particle Characteristics at Impact and Resultant Coating Properties

3.2.1 Porosity. Microstructural defects can be created when molten droplets impact and solidify on the substrate or on the previously deposited lamellae. If the liquid fraction of the impacting particles is too small, the interstices, inherent features of the overlapping of impacted particles, are not completely filled by the particle liquid phase. Moreover, the accommodation of splats to the asperities of the underlying layers is poor, resulting in the incorporation of coating porosity. For a low extent of melting, $\Delta T = 120$ °C ($\Delta T = T_{particle} - T_{m,}$ where T_m is the melting point of TiO_2); increased particle velocity, from 199 to 293 m/s, resulted in increased coating open porosity, rising from 10.4 to 12.8%. The increase in velocity broadens the temperature distribution, especially below the melting temperature, increasing the incorporation of particles in a plastic state and therefore, the porosity.

On the other hand, increases in molten particle temperature bring about decreasing particle viscosity at impact. Consequently, spreading of the molten particles is enhanced and the interstices can be better filled, involving decreasing coating open porosity. However, as shown in Table 3, if the particle velocity is too high, the low viscosity of the particle at impact leads to a splashing phenomenon and the coating open porosity value increases again.

In the case of IPS operating in the supersonic mode, the particle velocities increasing involves higher kinetic energy particles at point of impact. Consequently, despite the lower extent of melting, the deformation of particles at impact is increased and open porosity decreases again, as presented in Fig. 6.

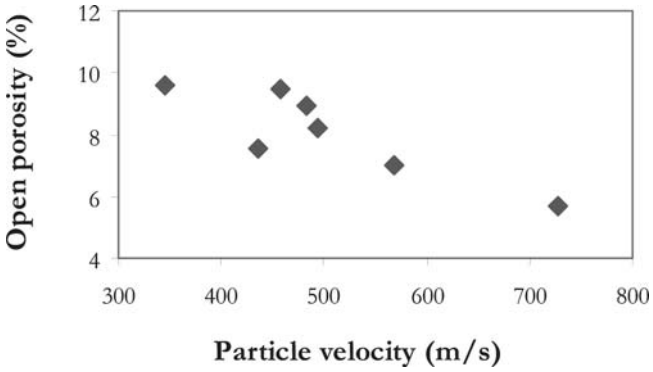

Fig. 6 Effect of particle velocity on the open porosity of IPS-supersonic coatings

Table 3 Effect of particles in-flight characteristics on the open porosity of APS coating

ΔT, °C ($\Delta T = T_{particle} - T_m$ TiO_2)	Particle velocity, m/s	Open porosity, %
120	199 ± 30	10.4
	293 ± 35	12.8
520	177 ± 20	5.6
	260 ± 30	9.0

3.2.2 Stoichiometry. The lightness of coatings that characterizes their stoichiometry, is mainly influenced by the particles temperature (Fig. 7).

This phenomenon is clearly highlighted in the case of APS coatings. Despite the substitution of hydrogen by helium in the plasma-forming gas mixtures, coatings were always gray in color, indicating reduction of titania particles during the spray process. The increased oxygen loss is related to increased particle temperature.

The quantitative evaluation of the APS coating stoichiometry shows that the ratio [O]/[Ti] ranged between 1.83 and 1.99 (the minimal ratio was obtained with the use of hydrogen as the plasma-forming gas). These ratios are close to the ratio for stoichiometric titania, explaining why the structure observed in the XRD pattern is predominantly the rutile phase. However, as seen in Fig. 8, some XRD peaks, corresponding to anatase, are also present.

Moreover, a broadening of the base of the rutile phase main peak ($2\theta = 27.4°$) can be observed. This can correspond to the presence of TiO_{2-x} phases, explaining the gray color of the coatings and variations in the gray density observed in optical micrographs, as shown in Fig. 9.

Comparison between IPS and APS coatings shows that, for similar particle temperatures at impact, the lightness value of the IPS coating was higher than that of the APS one. To explain the difference, the coatings were observed by their cathodoluminescence, CL (Ref 23). This method, frequently used for semiconductors (SC), is appropriate for this study because the oxygen loss leads to coatings with semiconductor behavior.

In Fig. 10, the IPS coating exhibits a less luminous response due to a smaller number of SC zones contrary to the APS one.

In the case of the IPS coating, lower particle velocities result in longer residence times for particles in the gas flow that con-

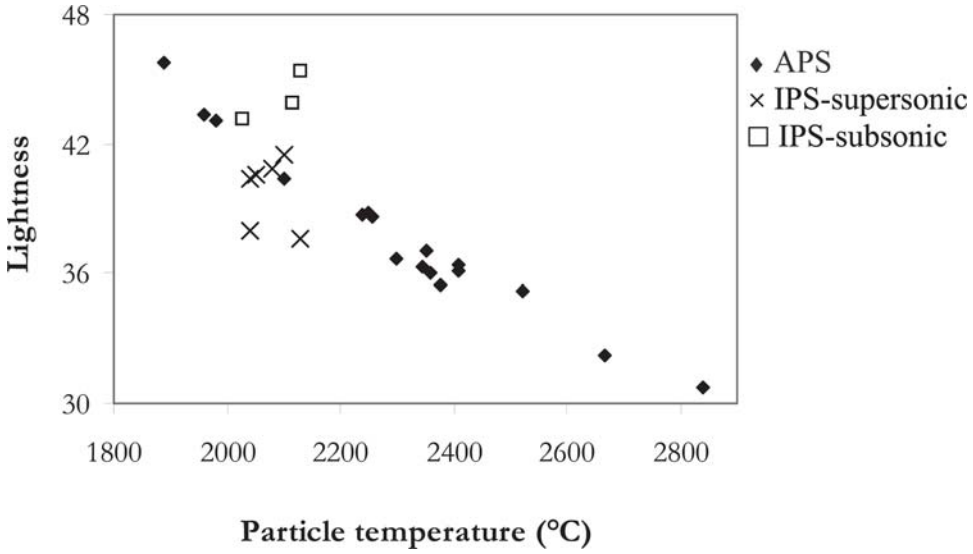

Fig. 7 Lightness value of coatings as a function of particles surface temperature at impact

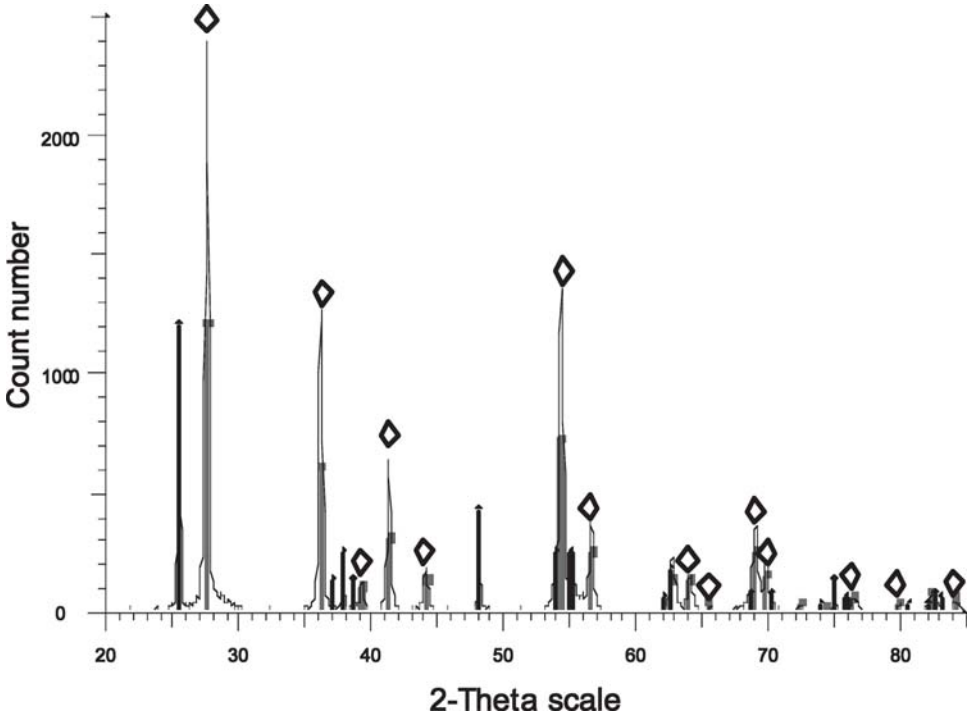

Fig. 8 XRD pattern of APS TiO_2 coating (◇ = rutile; other peaks = anatase)

tains oxygen (sheath gas). Consequently, the particles oxygen loss is compensated, thus explaining why coatings present less semiconductor zones.

3.2.3 Electrical Properties. In this section, the electrical properties will be linked to coating microstructure porosities and interlamellar contacts. Unfortunately, such measurements have not yet been performed on supersonic IPS.

As seen in Fig. 7, an increase in particle temperature leads to a more nonstoichiometric coating, resulting in a n-type semiconductor behavior (Fig. 2). Also, higher particle temperatures correspond to a better melted state of such particles on impact, resulting in a coating with fewer defects and, hence, of lower electrical resistivity. As can be seen in Fig. 11, the APS coatings with the lowest electrical resistivity values exhibited the weakest lightness value and the highest particle temperature.

Stoichiometry and porosity are both dependent on particle temperature. However, it is not easy to distinguish the effect of the one relative to the other. So, to better understand the influence of microstructure on the electrical resistivity, the variation of this property with the corresponding lightness value is drawn

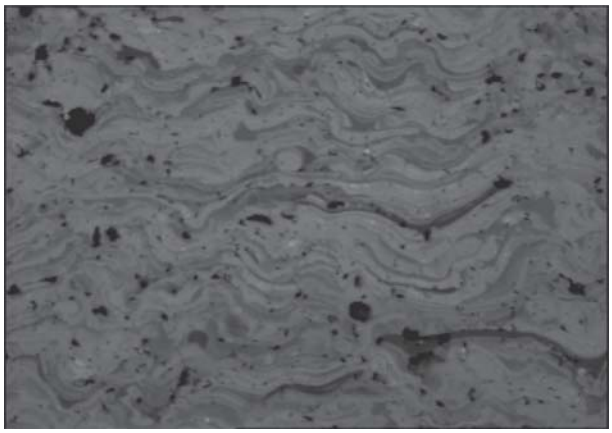

Fig. 9 Optical micrograph of APS TiO_2 coating

in Fig. 12. First, it may be noticed that the electrical resistivity increases with the lightness value. Indeed, an increase in the lightness value corresponds to titania coatings that have a more stoichiometric composition, and consequently, behave as an electrical insulator (Fig. 2). Secondly, for a given lightness value, the IPS coatings (obtained in both subsonic and supersonic modes) are less resistive than the APS ones.

In fact, the differences in particle velocity and temperature (Table 2) resulted in quite different coating microstructures. The lower impact velocities of particles sprayed with IPS in subsonic mode generated coating morphologies with a marked lamellar structure and composed of thick lamellae (a few micrometers compared with about 1 μm for APS) as evidenced by the fracture surface images of coatings shown in Fig. 13.

The APS coatings have a more chaotic microstructure and the contact areas between splats are more limited. In fact, in APS, the mean splat thickness is about 1 μm compared to 3 μm for the IPS-subsonic case. It can be assumed that a 3 μm thick splat obtained in the IPS process is equivalent to 3 splats obtained in APS by presenting a thickness of 1 μm but with a contact area of 100%. Contrary to the APS and supersonic IPS cases, the splat thickness is about 1 μm, but the contact area between them is only in the 30% range. Thus, for a coating thickness of 300 μm in both cases, the APS coating corresponds to the layering of 300 splats with a mean contact area of 30% while for the IPS coating, the same thickness corresponds to the layering of 100 splats with a 30% contact area and the layering of 200 splats with a perfect contact area, resulting in a mean contact area of $\{[(100 \times 0.3) + (200 \times 1)]/300\} \times 100 = 69\%$.

The interlamellar contacts have been experimentally observed by means of the infiltration of coatings with a fluorescent resin that makes it possible to enhance the microstructural features. Figure 14 shows an image, obtained by confocal laser scanning microscopy (CLSM), of two plasma-sprayed coatings.

As seen in Fig. 14, the fluorescent resin is observed to have penetrated the entire coating thickness, reaching as far as the interface between substrate and coating. It reveals the interconnected network of microstructural defects (porosity, cracks, poor interlamellar contacts). This confirms the hypothesis stated above, namely, that APS coatings exhibit higher densities of structural defects that can subsequently form obstacles to the transport of charge carriers involved in the electrical current conduction.

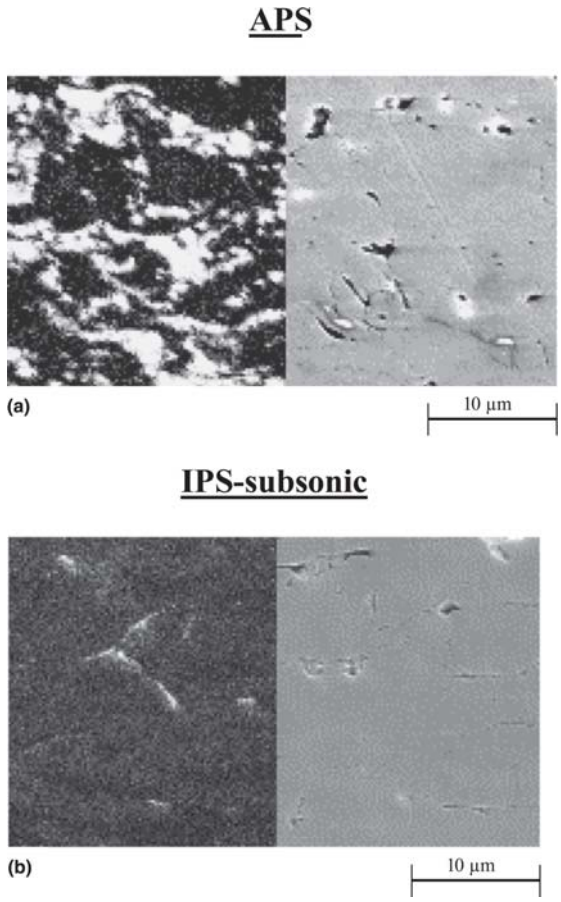

Fig. 10 CL (top) and SEM (bottom) micrographs of TiO_2 coatings prepared by APS and IPS-subsonic

Moreover, for the same coating thickness, IPS-subsonic mode coatings contain fewer splats, and, consequently, the number of electrically resistive interfaces throughout the coating is decreased. This observation has already been made in the case of the thermal properties of plasma-sprayed coatings: the thermal diffusivity of tungsten plasma-sprayed coatings was increased when the individual lamellae were thicker (Ref 4).

Moreover, the comparison between the IPS and APS coatings that have about the same lightness values (i.e., the number of charge carriers throughout both coatings is about the same) has permitted a better understanding of the coating microstructure effects to be obtained. Table 4 summarizes the properties of these coatings presenting similar lightness values.

Open porosity is apparently not the principal parameter involved in the modification of coating electrical properties, particularly, if those coatings, whose lightness value is around 38.5, are compared. The IPS-subsonic coating with the higher percentage of open porosity presents the lower values of electrical resistivity. The microstructure of the plasma-sprayed coatings consists of a stack of lamellae that can contain porosity and imperfect interlamellar contacts. As the open porosity was found not to be a relevant parameter, their microporosity has been investigated using the mercury intrusion method. It has been found that the APS coating ($L = 38.6$) exhibited pore diameters around 60 nm, whereas the IPS coating did not present any microporosity as much pronounced, as shown in Fig. 15.

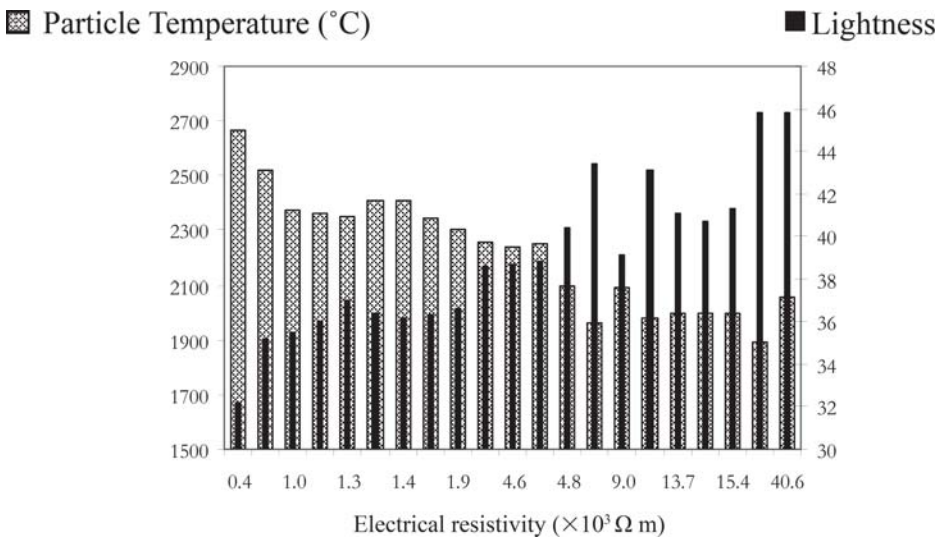

Fig. 11 Variation of APS TiO_2 coatings electrical resistivity with particle temperature at impact (white bar) and lightness value (black bar) of coatings

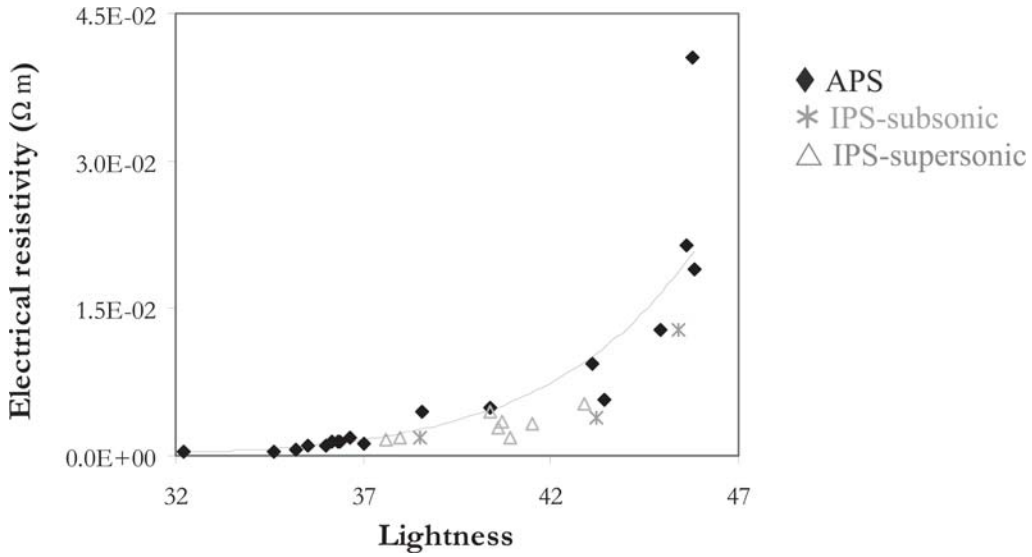

Fig. 12 Relationship between electrical resistivity and lightness value of coatings for the three spraying processes used in the study

Furthermore, the comparison of the two metallographic connections presented in Fig. 16 shows that, despite a more marked lamellar structure, the IPS coating tends to exhibit a lower resistivity than the APS coating. To eliminate the effect of the substrate temperature, it would be interesting to investigate the IPS-supersonic coatings with the same characterizations (MEB, CL, CLSM, mercury porosity). Indeed, as explained in the experimental procedure, in the IPS installation, the deposition temperature varied between 400 and 500 °C, depending on the operating conditions of the spray process. It is well known that the deposition temperature of the growing coating strongly affects the microstructure and the related defect structure. At high temperatures, the contact zone between splats is enhanced and the number of structural defects decreases (Ref 24). Akani et al. (Ref 25) demonstrated that varying the substrate temperature from 450 to 1100 °C involves decreases in the electrical resistivity of plasma-sprayed silicon coatings by ~5 orders of magnitude.

4. Conclusions

This work deals with a better understanding of the correlation between the microstructure and electrical properties of plasma-sprayed coatings. The material studied is titania, whose electrical properties are very sensitive to the plasma-spraying parameters.

The experimental approach has involved the use of two plasma spray processes: APS and inductive plasma spraying (IPS in a controlled atmosphere at a pressure lower than APS) that have permitted a broad range of particle temperatures and velocities to be obtained at impact and thus, coatings with quite different microstructures. Measurements of particle velocity and

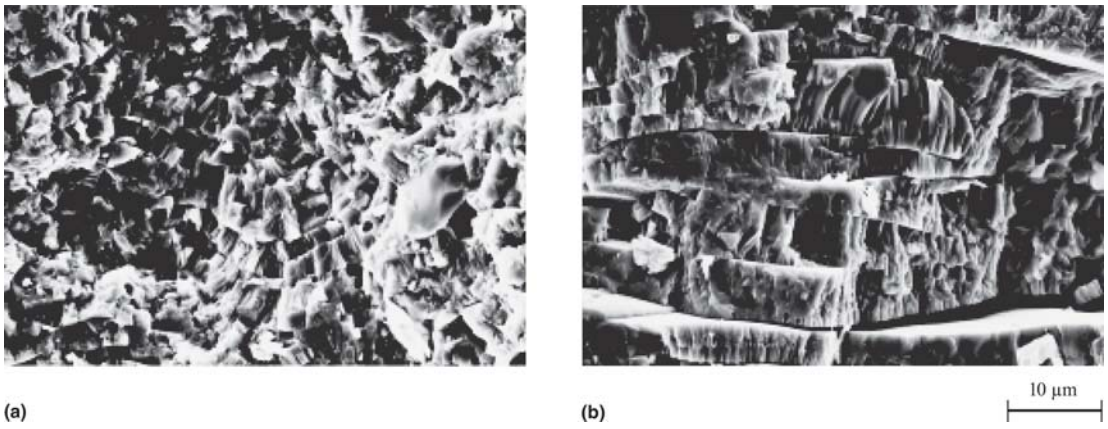

Fig. 13 Fracture surfaces of the as-sprayed TiO_2 coatings (a) APS (22-45 μm); (b) IPS-subsonic

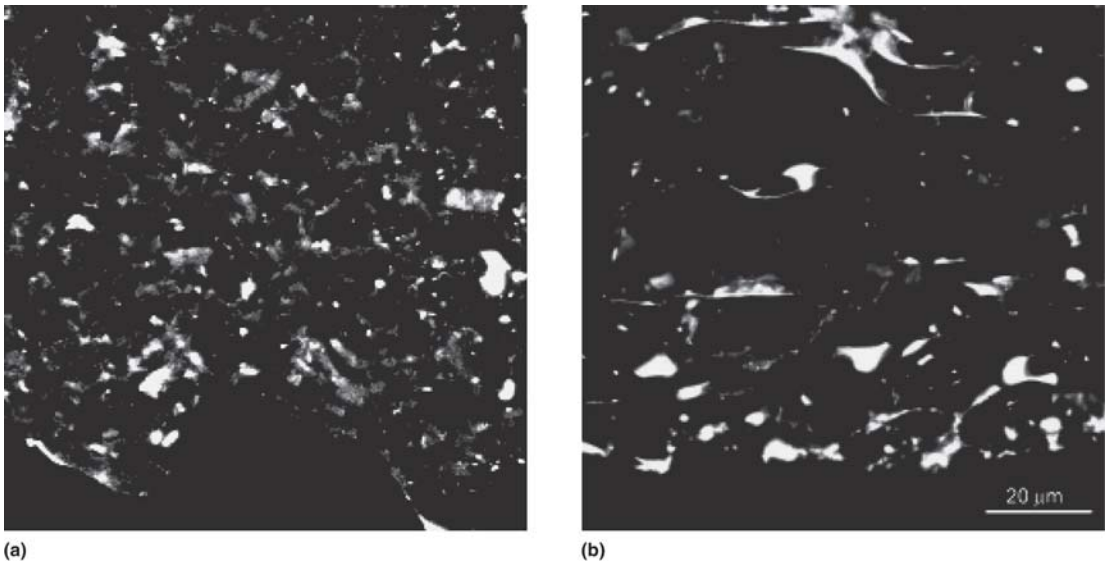

Fig. 14 CLSM image of plasma-sprayed titania coatings: (a) APS, (b) IPS-subsonic. The magnification is the same for both micrographs

Table 4 Properties of coatings sprayed by APS and IPS presenting similar lightness values

Spraying process	Lightness value (L)	Electrical resistivity (ρ) Ω m	Open porosity (P) %	Apparent density
IPS	38.5	1.8×10^{-3}	6.3	4.00
APS	38.6	4.5×10^{-3}	5.9	3.93
IPS	43.2	3.9×10^{-3}	7.2	3.95
APS	43.1	9.4×10^{-3}	12.8	3.57
IPS	45.4	12.9×10^{-3}	11.2	3.78
APS	45.8	19.0×10^{-3}	11.0	3.69

temperature have made it possible to link the plasma operating parameters and the in-flight particle characteristics prior to impact on the substrate. For example, the chamber pressure used for the IPS process was found to be the factor that most affects the particle velocity.

Despite the corrected stoichiometry of the starting powder, all coatings obtained were gray in color, thus revealing a loss of oxygen during the spray process. This loss was higher when the particle temperature increased. Through cathodoluminescent

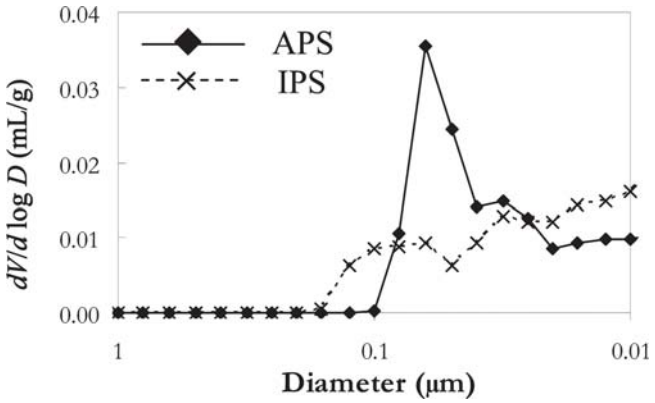

Fig. 15 Pore size distribution of APS and IPS-subsonic coatings presenting a lightness value L of 38.5

analysis of the titania plasma-sprayed coatings, it was observed that adding oxygen to the IPS spray process was not on its own sufficient to limit the decomposition of titania. The oxygen gas

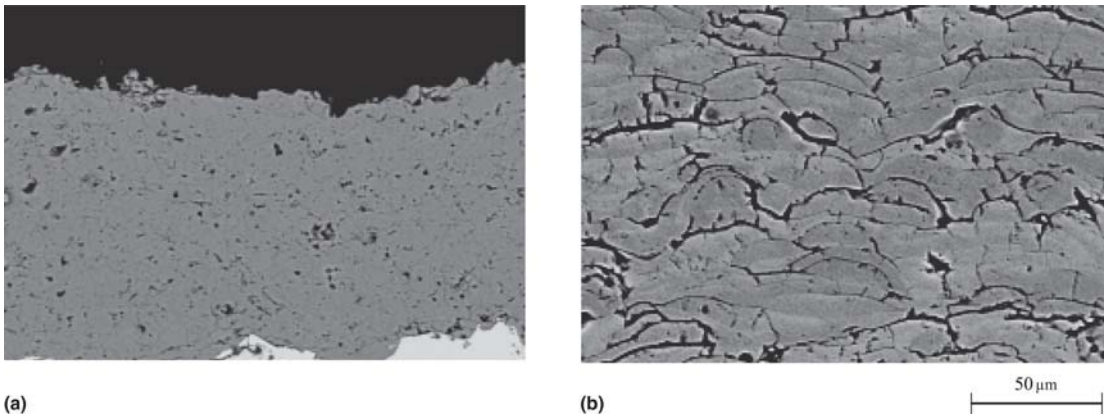

Fig. 16 Cross sections of TiO_2 coatings with similar lightness value L and open porosity P but of different electrical resistivity, ρ: (a) APS, $L = 45.8$, $P = 11.0\%$, $\rho = 19.0 \times 10^{-3}$ Ω m; (b) IPS, $L = 45.4$, $P = 11.2\%$, $\rho = 12.9 \times 10^{-3}$ Ω m

addition must be combined with a low particle velocity, obtained under subsonic IPS conditions, to favor chemical equilibrium between the particle and the plasma environment.

The isolation of the stoichiometry influence has permitted the demonstration of the fact that the interlamellar contacts strongly affect the electrical resistivity. Moreover, comparison between the APS and IPS coatings highlights the effect of the distance between structural defects. Indeed, if the distance between structural defects was of the same order as the mean free path of charge carriers, the electrical resistivity would be increased. However, even if there are less defects, the quality of the contacts must be as good as possible to permit the transport of charge carriers through the coating.

The influence of the quality of contacts as well as the coating temperature should be studied in more details. The IPS supersonic coatings with thin splats obtained at impact velocities between 300 and 600 m/s should give interesting trends. However, as for IPS subsonic coatings, the experimental set-up should be modified to allow a careful control of the mean coating temperature during deposition.

References

1. P. Fauchais and A. Vardelle, Thermal Plasmas, *IEEE Trans. Plasma Sci.,* 1997, 25, p 1258-1280
2. S. Sampath, X.Y. Jiang, J. Matejicek, A.-C. Léger, A. Vardelle, Substrate Temperature Effects on Splat Formation, Microstructure Development and Properties of Plasma Sprayed Coatings—Part I: Case Study for Partially Stabilized Zirconia, *Mater. Sci. Eng.,* 1999, A272, p 181-188
3. L. Pawlowski and P. Fauchais, Thermal Transport Properties of Thermally Sprayed Coatings, *Int. Mater. Rev.,* 1992, 37 (6), p 271-289
4. S. Boire-Lavigne, C. Moreau, and R.G. Saint-Jacques, The Relationship Between the Microstructure and Thermal Diffusivity of Plasma-Sprayed Tungsten Coatings, *J. Thermal Spray Technol.,* 1995, 4 (3), p 261-267
5. S. Safai, "A Microstructural Investigation of Plasma-Sprayed Metal and Oxide Coating," Ph.D. dissertation, Stony Brook University, New York, 1979
6. A. Ohmori, K.-C. Park, M. Inuzuka, K. Inoue, N. Iwamoto, Electrical Conductivity of Plasma-Sprayed Titanium Oxide (Rutile) Coatings, *Thin Solid Films,* 1991, 201, p 1-8
7. J. Takeuchi, R. Yamasaki, and Y. Harada, Development of a Low-Pressure Plasma Sprayed Ceramic Coating on Electrostatic Chucks for Semiconductor Manufacturing Equipment, *Proceedings of the ITSC 2002,* E. Lugscheider, Ed., DVS Publishing House, Düsseldorf, Germany, 2002, p 960-964
8. M.I. Boulos, RF Induction Plasma Spraying: State-of-the-Art Review, *J. Thermal Spray Technol.,* 1992, 1 (1), p 33-40
9. H.C. Chen and E. Pfender, Microstructural Comparison of Alumina Coatings Prepared by RF and DC Plasma Spraying, *Proceedings of UTSC 99,* E. Lugscheider, P.A. Kammer, Ed., DVS Publishing House, Düsseldorf, Germany, p 603-607
10. K. Mailhot, F. Gitzhofer, and M.I. Boulos, Supersonic Induction Plasma Spraying of Dense YSZ Electrolyte Membranes, *Thermal Spray: A United Forum for Scientific and Technological Advances,* C.C. Berndt, Ed., ASM Int., 1997, p 21-24
11. R. Henne, V. Borck, M. Muller, R. Ruckdaschel, and G. Schiller, New applications and new product qualities by RF plasma spraying, *Proceedings of the United Thermal Spray Conference 99,* E. Lugscheider, P.A. Kammer, Ed., DVS Publishing House, Düsseldorf, Germany, 1999, p 598-602
12. P. Fauchais, A. Vardelle, and B. Dussoubs, Quo Vadis Thermal Spraying, *J. Thermal Spray Technol.,* 2001, 10 (1), p 44-66
13. N. Branland, E. Meillot, P. Fauchais, A. Vardelle, F. Gitzhofer, and M.I. Boulos, Relationships Between Microstructure and Electrical Properties of Plasma-Sprayed TiO_2 Coatings, Part F, *Surface Engineering with Ceramics, Proceedings of CIMTEC* 2002—Florence, Italy, P. Vincenzini, Ed., Techna Group Srl, 2002
14. C. Moreau, P. Gougeon, M. Lamontagne, V. Lacasse, G. Vaudreuil, P. Cielo, On-Line Control of the Plasma Spraying Process by Monitoring the Temperature, Velocity and Trajectory of In-Flight Particles, *Thermal Spray Industrial Applications,* C.C. Berndt and S. Sampath, Ed., ASM. Int., 1994, p 431-437
15. S.D. Glancy, Preserving the Microstructure of Thermal Spray Coatings, *Adv. Mater. Process.,* 1995, 7, p 37-40
16. A.R. Spurr, A Low-Viscosity Epoxy Resin Embedding Medium for Electron Microscopy, *J. Ultrastruct. Res.,* 1969, 26, p 31-43
17. N. Llorca-Isern, M. Puig, and M. Español, Improving the Methodology for Coating Defects Detection, *J. Thermal Spray Technol.,* 1999, 8 (1), p 73-78
18. E.J. Garboczi, Mercury Porosimetry and Effective Networks for Permeability Calculations in Porous Materials, *Powder Technol.,* 1991, 67, p 121-125
19. G. Wyszecki and W.S. Stiles, *Color Science: Concepts and Methods, Quantitative Data and Formulae,* 2nd ed., Wiley, New York, 1982
20. J. Laplume, Bases Théoriques de la Mesure de la Résistivité et de la Constante de Hall par la Méthode des Pointes, *Onde Electr.,* 1955, 335, p 113-125
21. N. Branland, "Plasma Spraying of Titania Coatings: Contribution to the Study of Their Electrical Properties and Microstructures," Ph.D. dissertation, University of Limoges, France/University of Sherbrooke (Canada), 2002 (in French)
22. M. Vardelle, A. Vardelle, and P. Fauchais, Spray Parameters and Particle Behavior Relationships During Plasma Spraying, *J. Thermal Spray Technol.,* 1993, 2 (1), p 79-92
23. V.I. Petrov, Cathodoluminescence Scanning Microscopy, *Phys. Status Solidi,* 1992, 133, p 189-230
24. P. Bengtsson and T. Johannesson, Characterization of Microstructural Defects in Plasma-Sprayed Thermal Barrier Coating, *J. Thermal Spray Technol.,* 1995, 4 (3), p 245-251
25. M. Akani, R. Suryanarayanan, and G. Brun, Influence of Process Parameters on the Electrical Properties of Plasma-Sprayed Silicon, *J. Appl. Phys.,* 1986, 60 (1), p 457-459